RESEARCH ARTICLE

Check for updates

Metal–organic macrocycles with tunable pore microenvironments for selective anion transmembrane transport†

Yingguo Li, [ID] Lei Jia, Xianhui Tang, [ID] Jinqiao Dong, Yong Cui [ID] and Yan Liu [ID] *

The development of artificial ion channels is critically important not only for understanding the natural processes but also for many applications. Exploring how to finely tune the pore microenvironments is the key to achieving highly efficient synthetic ion channels. Here we report the self-assembly of a distinct type of four-membered metallacycles with tunable pore microenvironments capable of selective anion transmembrane transport. By elaborately designing three 1,1'-bi-2-naphthol-based ligands, we prepare three cationic Zn_4L_4 metallacycles with sub-nanosized apertures. In this system we can finely tune the pore sizes and binding sites through the deployment of pre-designed ligands with hydroxyl, ethoxyl, and pentaethylene glycol groups. We found that the metallacycle with hydrophilic hydroxyl moieties is unable to transport anions owing to its low lipophilicity, whereas the one bearing pentaethylene glycol units can transport the anions but with low selectivity. In contrast, the analogous metallacycle featuring ethoxyl groups and hydrophobic pore surfaces displays a significantly higher transport efficiency for iodide ions over other monovalent anions, with I^-/X^- selectivities of up to 38. Our finding unambiguously reveals that the transport abilities of self-assembled complexes are highly dependent on their pore microenvironments.
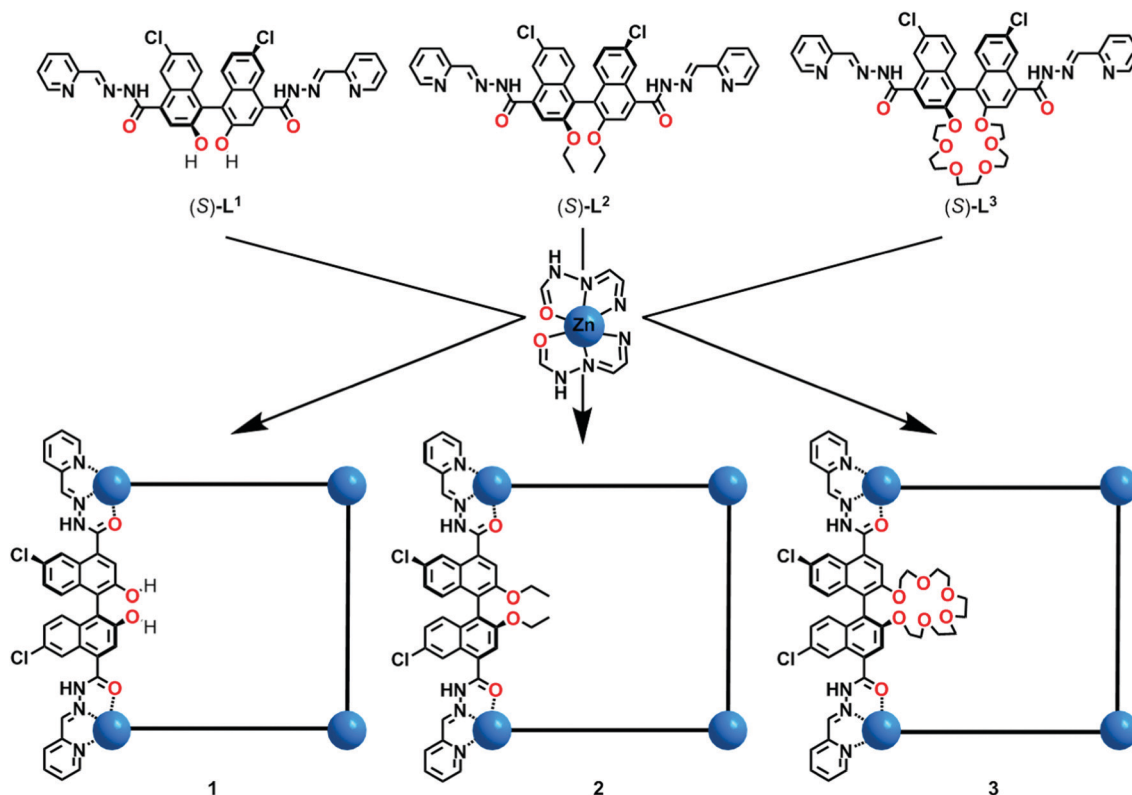
Introduction

In living cells, ion transport across biomembranes regulated by ion channels is essential for them to live.[1,2] Inspired by natural ion channels, the design and development of synthetic ion channels is extremely important not only for the deep understanding of the transport process,[3–6] but also for their potential applications in sensing,[7] catalysis,[8] drug discovery,[9] and nanotechnology.[10] The flow of ions is a typical supramolecular process, which requires specific ion-channel interactions for compensating the loss of hydration energy and stabilizing the dehydrated ions when crossing the phospholipid bilayer.[11] Along this line, a large number of synthetic ion channels and pores have been designed for transporting K^+, Cl^- and I^-.[12–14] The majority of them are assembled from organic molecules such as crown ethers,[15] cyclic peptides,[16] and rigid-rod β-barrels.[17] For many applications, particularly in the field of separation and catalysis,[18–21] thermo-dynamically and kinetically stable structures forming well-defined and rigid pores in

the membrane are strongly desired. However, the design of highly ion-selective channels, which can compare well with natural systems, remains a grand challenge, presumably because it is hard to chemically tune a mimic pore with well-arranged binding sites and a suitable hydrophobic effect at the molecular level.[22–24]

Porous metal–organic/organic assemblies, such as macrocycles and cages, possess intrinsic nanocavities with multiple open windows, which have been widely investigated for their aesthetic architectures[25–28] and diverse applications.[29–33] Perhaps most importantly, recent studies showed that these supramolecular assemblies hold great promise as synthetic channels to selectively translocate anions, cations and even small molecules in lipid systems.[34–39] For instance, Fyles *et al.* proposed that self-assembled metal–organic macrocycles can serve as synthetic ion channels.[40] Kim *et al.* demonstrated that a porphyrin-based organic cage capable of a large cavity can function as an iodide-selective channel.[41] Nitschke and Keyser *et al.* found that a pentagonal $Zn_{10}L_{15}$ prism with a channel-like cavity is capable of forming blockable long-lived Cl^- channels within lipid bilayer membranes.[42] Although this concept has been demonstrated by these meritorious examples, the design and synthesis of artificial ion channels with high selectivity is still challenging and requires special effort. To meet this challenge, the supramolecular assemblies need to possess a

School of Chemistry and Chemical Engineering, Frontiers Science Center for Transformative Molecules and State Key Laboratory of Metal Matrix Composites, Shanghai Jiao Tong University, Shanghai 200240, China. E-mail: liuy@sjtu.edu.cn

† Electronic supplementary information (ESI) available: Detailed experimental procedures and additional figures. CCDC 2103358. For ESI and crystallographic data in CIF or other electronic format see DOI: 10.1039/d2qm00065b

Scheme 1 Design and self-assembly of four-membered metallacycles 1–3.

superior pore microenvironment, where it is capable of specifically positioned binding sites, complementary size and shape between the host and guest, and controllable pore surfaces.[43–49] All these considerations are key to achieving synthetic ion channels with high selectivity.[50–54]

With this context in mind, we develop a new system for self-assembly of well-defined shape-persistent metallacycles based on the 1,1′-bi-2-naphthol (1,1′-BINOL)-derived skeleton. Specifically, three cationic Zn_4L_4 metallacycles are designed to feature well-arranged hydroxyl, ethoxyl or pentaethylene glycol groups (Scheme 1). As we expected, the pore microenvironments within the metallacycles involving cavity sizes, binding sites, and hydrophobic surfaces can be precisely tuned through the deployment of the deliberately selected (S)-BINOL-derived ligands. It has been suggested that the binding affinities and transmembrane transport abilities of these supramolecular assemblies are significantly influenced by their chemical microenvironments, as unambiguously revealed by extensive experiments. We found that metallacycle 1 bearing hydrophilic hydroxyl groups is unable to transport anions through a bilayer membrane resulting from its low lipophilicity, while metallacycle 3 containing pentaethylene glycol groups can transport anions but with low selectivity due to the amphiphilic pore surfaces. In sharp contrast, the analogous metallacycle 2 featuring hydrophobic ethyl groups can efficiently transport anions, with I^-/X^- transport selectivities of up to 38 which is comparable to those of the reported state-of-the-art supramolecular anion transport systems.[13,41]

Results and discussion

Synthesis and characterization

The ligand (R/S)-L^1 was prepared by a Schiff-base reaction of 6,6′-dichloro-2,2′-dihydroxy-[1,1′-binaphthalene]-4,4′-dicarbohydrazide and 2-pyridylaldehyde in one step with a 94% yield. (R/S)-L^2 and (R/S)-L^3 were prepared by a similar procedure with 73% and 88% yields, respectively. Crystalline samples of the metallacycles were prepared by reacting (R/S)-L^{1-3} and $Zn(ClO_4)_2$ with a molar ratio of 1:1 in acetonitrile at room temperature (Scheme 1). Single crystals of $[Zn_4L^2_4]\cdot 8ClO_4$ were obtained by the liquid diffusion of (S)-L^2 and $Zn(ClO_4)_2$ in dioxane/methanol solution with a 54% yield. The products were characterized using a variety of techniques including single-crystal X-ray diffraction, IR spectroscopy, UV-Vis spectroscopy, nuclear magnetic resonance (NMR), and electrospray ionization mass spectrometry (ESI-MS).

The ^{1}H and ^{13}C NMR spectra of each metallacycle displayed only one set of ligand resonances in solution, indicating the formation of a single species by self-assembly of L and $Zn(ClO_4)_2$ (Fig. 1a–c and Fig. S1–S8, ESI†). The C_2-symmetry of BINOL units was preserved in all cases, as can be deduced from the number of proton signals. The ^{1}H diffusion-ordered NMR spectroscopy (DOSY) spectrum of each metallacycle displayed a single set of signals as well, further suggesting the formation of a single product. The comparable measured diffusion coefficients of $D = 4.17 \times 10^{-10}$ m^2 s^{-1} for the three assemblies (corresponding to a hydrodynamic radius of $\sim$13.9 Å) were indicative of their analogous sizes and shapes.

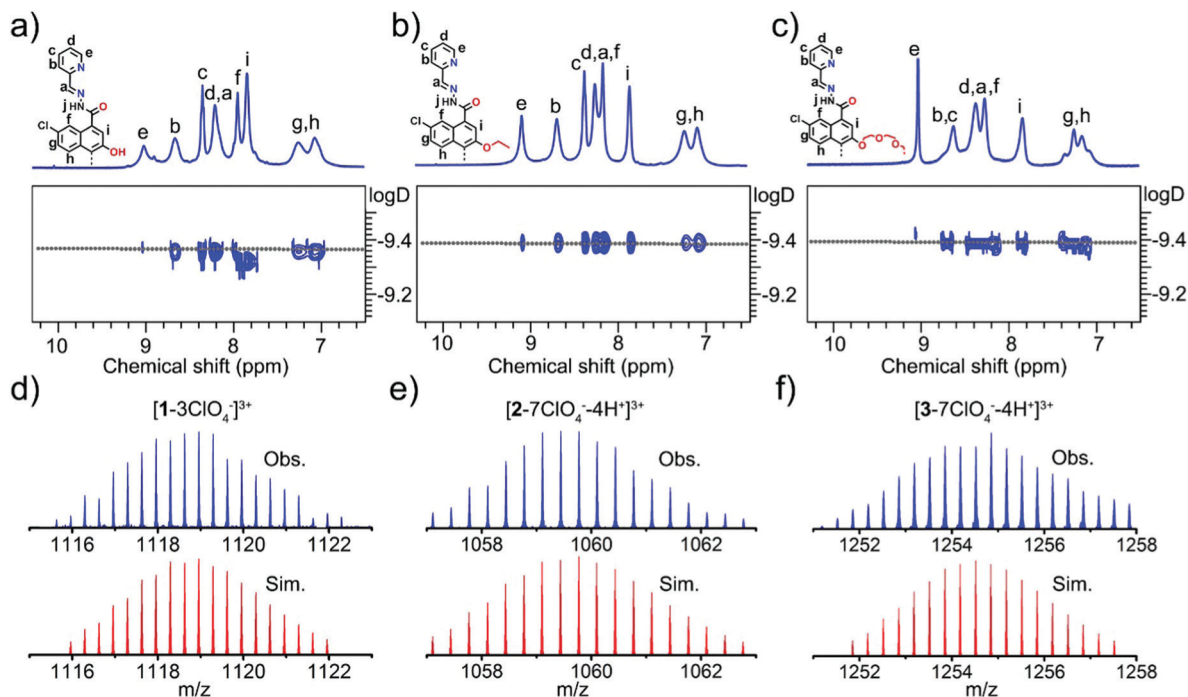**Fig. 1** (a−c) Partial ^{1}H NMR and 2D DOSY spectra (500 MHz, CD$_3$CN, 298 K) of **1**–**3**. (d−f) Experimental ESI-MS and calculated isotope patterns of **1**–**3**.

The formation of tetrametallacycles was further confirmed by high-resolution ESI-MS. For example, two distinct peaks at m/z = 1085.3119 and 1118.9598 were observed in metallacycle 1, which can be assigned to $[\mathbf{1}-4ClO_4^- -H^+]^{3+}$ and $[\mathbf{1}-3ClO_4^-]^{3+}$, respectively (Fig. 1d and Fig. S3, ESI†). Metallacycle 2 displayed a group of prominent signals at m/z = 1026.1225, 1059.7734 and 1093.0120 which belong to $[\mathbf{2}-8ClO_4^- -5H^+]^{3+}$, $[\mathbf{2}-7ClO_4^- -4H^+]^{3+}$ and $[\mathbf{2}-6ClO_4^- -3H^+]^{3+}$ species, respectively (Fig. 1e and Fig. S6, ESI†). Metallacycle 3 exhibited several peaks at m/z = 733.1217, 741.9145, 750.7017 and 1254.8511, corresponding to $[\mathbf{3}-8ClO_4^- -3H^+]^{5+}$, $[\mathbf{3}-8ClO_4^- -5H^+ + 2Na^+]^{5+}$, $[\mathbf{3}-8ClO_4^- -7H^+ + 4Na^+]^{5+}$ and $[\mathbf{3}-7ClO_4^- -4H^+]^{3+}$, respectively (Fig. 1f and Fig. S9, ESI†). All these peaks agree well with the simulated and the natural isotopic abundances.

Single-crystal X-ray diffraction revealed that 2 crystallizes in the chiral orthorhombic $C222$ space group with two Zn ions (located on the twofold axis), one (S)-$\mathbf{L}^2$ and two ClO$_4^-$ in the asymmetric unit. The tetrametallic structure is composed of four linear (S)-$\mathbf{L}^2$ linkers and four six-coordinated Zn^{2+} ions in an alternating fashion with an ideal D_2 symmetry (Fig. 2a). Four N$_2$O–Zn nodes located in the vertices are linked by four linear (S)-$\mathbf{L}^2$ linkers to form a cation square-like metallacycle with the formula of $[Zn_4L_4^2]\cdot(ClO_4)_8$, and the positive charges are balanced by eight ClO$_4^-$. The four (S)-$\mathbf{L}^2$ are positioned on the parallel edges of the metallacycle square, and each zinc ion is coordinated in a *mer*-position with two N$_2$O chelators. The Zn–N and Zn–O bond lengths are 2.10 (2) and 2.23 (3) Å, respectively, which are in good agreement with typical Zn complexes.[33] The adjacent and opposite Zn···Zn separations are 15.65 Å and 22.26 Å, respectively. The square macrocycle

has an outer diameter of 28.22 Å and a height of 12.31 Å (Fig. S11, ESI†), and a central pore diameter of 6.01 Å (Fig. 2b). Two pairs of ethoxyl groups and naphthyl rings of the four (S)-$\mathbf{L}^2$ are organized such that they partly cover two sides of the metallacycle along the C_2-axis, thereby generating a hydrophobic open cavity with a diameter of 6.01 Å, which is large enough to encapsulate and transport small guests. Packing of metallacycles in parallel along the crystallographic c-axis leads to one-dimensional interrupted tubular channels with a central opening of 6.0 × 6.3 Å flanked by two 4.0 × 6.0 Å pores, in which two adjacent metallacycles are held together by strong electrostatic interactions between two pairs of tetrametallic cations and ClO$_4^-$ counteranions (Fig. 2c). The ClO$_4^-$ anions, which are located around the metal vertices, direct the tubules to produce a porous structure through cation–anion contacts. The structure is reinforced by intermolecular π–π (plane-to-plane separation of 3.59 Å) and CH···π (3.24–3.51 Å) interactions (Fig. 2d and Fig. S12, ESI†). Therefore, highly directional noncovalent interactions in **2** have steered the packing of metallacycles into a three-dimensional supramolecular tubular framework (Fig. S13, ESI†). The calculations utilizing PLATON show that the cationic framework has about 57.1% of the total volume available for solvent molecules.[55]

Great attempts have been made to grow single crystals of **1** and **3** suitable for X-ray diffraction, but failed. Subsequently, we performed molecular simulations to build molecular models for them by DFT calculations. As the backbone and length of (S)-$\mathbf{L}^1$ and (S)-$\mathbf{L}^3$ are similar to those of (S)-$\mathbf{L}^2$, the energy-minimized structures show that assemblies **1** and **3** maintain the M$_4$L$_4$ square structure, in which four Zn centres adopt the same *mer* configurations to connect with four ligands in an
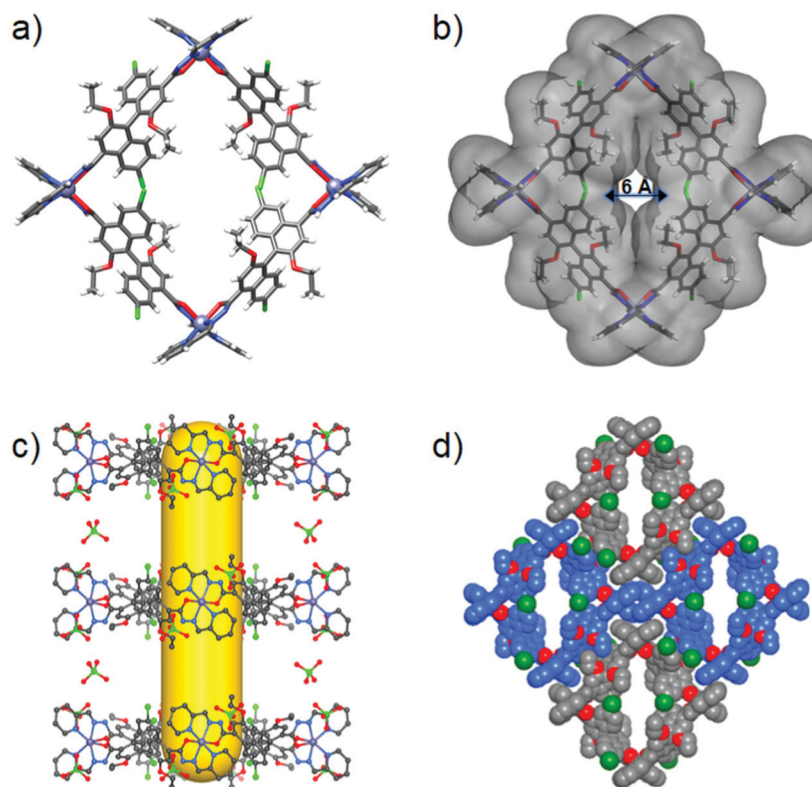
Fig. 2 (a) Single-crystal X-ray structure of **2**. (b) Solvent-accessible iso-surface model of **2** shown from the above. (c) Packing of **2** to generate a nanotube. (d) The extended structures are generated with four rings. Gray: C; red: O; green: Cl; white: H; dodger blue: N; light blue: Zn. The channel is highlighted by the yellow stick.

alternating fashion (Fig. 3a and b). **1** and **3** have an outer diameter of 28.22 Å, heights of 10.03 and 17.22 Å (Fig. S11, ESI†), and inner pore diameters of 9.54 and 6.51 Å, respectively (Fig. 3c and d). Obviously, the pore environments of metallacycles involving the cavity size and shape, recognition site, and surface nature can be finely tuned by employing organic linkers with different functionalities. To the best of our knowledge, metallacycle **2** is a rare example of a self-assembled molecular container with a narrow pore size that can pack into an ultramicroporous tubular structure (pore diameter < 0.7 nm),[56] which holds great potential for selectively transporting small ions and molecules.[3]

UV-vis spectroscopy enabled the quantification of the binding strengths of various halides and cations with metallacycles. Thus, the UV-vis titration experiments were performed with a fixed concentration of the metallacycle and ions at 5.0×10^{-6} M and 1.0×10^{-3} M in CH_3CN, respectively. Progressive addition of halides led to the gradual hypsochromic shift combined with a decrease in the intensity of the absorption band at ~ 378 nm for **1–3**, which is attributed to the interactions between the halide and metallacycle, along with the appearance of stable isosbestic points. We infer that the observed large blue shift and absorption weakening are a result of the conformational changes of (S)-BINOL units by the formation of host–guest binding. As shown in Fig. 4a–c and Fig. S14, (ESI†) when **1** was titrated with tetrabutylammonium chloride (TBACl),

tetrabutylammonium bromide (TBABr), tetrabutylammonium iodine (TBAI), tetrabutylammonium nitrate (TBANO$_3$) and tetrabutylammonium perchlorate (TBAClO$_4$), respectively, the absorption at 378 nm was weakened. The degree of weakening decreased in the order of $Cl^- > Br^- > I^- > NO_3^- > ClO_4^-$, indicating that **1** has a different binding capacity to Cl^-, Br^-, I^-, NO_3^- and ClO_4^- anions. The association constant (K_a) for complexation of **1** with halides was estimated based on *BindFit* with a 1:1 (host:guest) binding model.[57] Moreover, the stoichiometry of 1:1 was further confirmed by high-resolution mass spectrometry. For example, the peak at 1063.9875 can be assigned to $[1-5ClO_4^- - H^+ + Cl^-]^{3+}$, indicative of the 1:1 binding model between metallacycle 1 and the halide (Fig. S18, ESI†). The K_a constants were calculated to be 11.9×10^4, 8.6×10^4, 6.6×10^4 and 2.3×10^4 M^{-1} for Cl^-, Br^-, I^- and NO_3^-, respectively (Fig. S14 and Table S3, ESI†). However, the K_a constant of ClO_4^- cannot be accurately calculated because of its extremely weak binding capability. Halide-binding studies with **2** and **3** were also performed, affording $K_{2-Cl^-} = 7.6 \times 10^4$ M^{-1}, $K_{2-Br^-} = 6.8 \times 10^4$ M^{-1}, $K_{2I^-} = 4.6 \times 10^4$ M^{-1}, $K_{3-Cl^-} = 3.8 \times 10^4$ M^{-1}, $K_{3-Br^-} = 3.1 \times 10^4$ M^{-1}, $K_{3-I^-} = 1.9 \times 10^4$ M^{-1}, and $K_{3-NO3^-} = 1.2 \times 10^4$ M^{-1} (Fig. S15, S16 and Table S3, ESI†). Again, due to weak binding, the constants K_{2-NO3^-}, K_{2-ClO4^-} and K_{3-ClO4^-} cannot be determined. Obviously, the three metallacycles exhibit different anion binding behaviours in solution, but all followed the sequence of $Cl^- > Br^- > I^- >$

This journal is © The Royal Society of Chemistry and the Chinese Chemical Society 2022

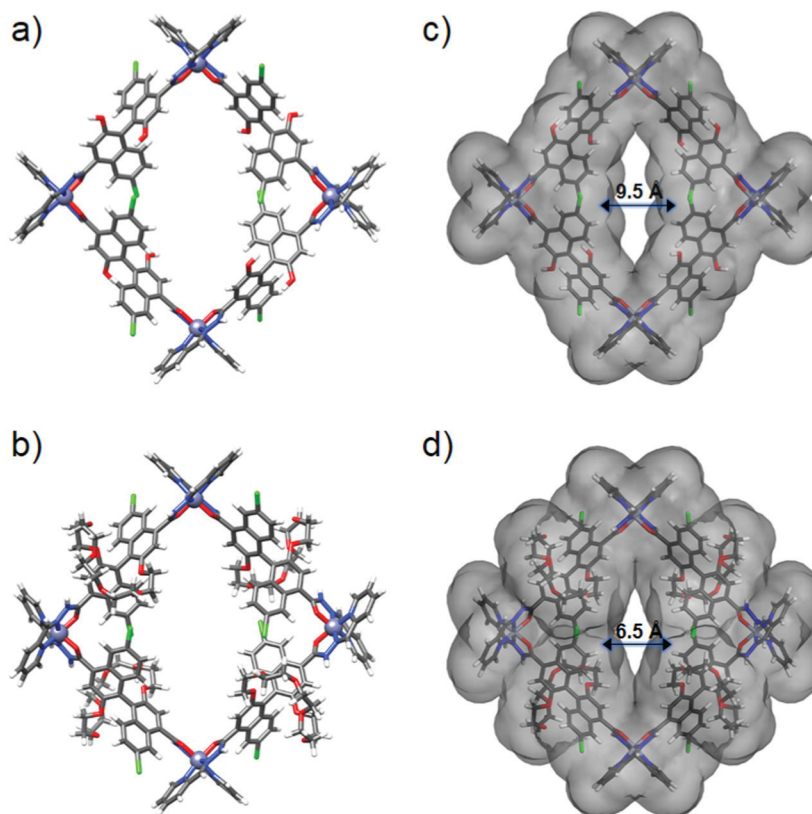*Mater. Chem. Front.*, 2022, **6**, 1010–1020 | **1013**

Fig. 3 (a and b) Energy-minimized conformations of **1** and **3** based on DFT calculations. (c and d) Solvent-accessible iso-surface models of **1** and **3** shown from the above. Gray: C; red: O; green: Cl; white: H; dodger blue: N; light blue: Zn.

NO_3^- > ClO_4^-, demonstrating their potential ability of ion recognition.

Under identical conditions, metallacycle **3** can also bind alkali metal ions, but with small association constants. For example, the constants of K_{3-Li}^+, K_{3-Na}^+, K_{3-K}^+ and K_{3-Rb}^+ were found to be 1302, 2293, 3237, and 1856 M^{-1}, respectively, which are much smaller than those of halide anions (Fig. S17 and Table S3, ESI†). The host–guest complex with K^+ has the largest K value among the four examined cations, which follows the size-fit rule that 18-crown-6 favours potassium ions.[58] The quite different binding selectivity of metallacycles to anions and cations showcased their potential as a channel to selectively transport ions through its unimolecular pathway.

Transmembrane transport of ions

The selective ion binding behaviors of **1–3** promoted us to explore their ion transport activity across the large unilamellar vesicles (LUVs).[37] We firstly investigated the ion-transport activity of the metallacycles by using the 8-hydroxypyrene-1,3,6-trisulfonate (HPTS) assay. The HPTS-containing vesicles were prepared from the egg yolk phosphatidylcholine (EYPC) lipid in 4-(2-hydroxyethyl)-1-piperazine ethanesulfonic acid (HEPES) buffer ([HEPES] = 10 mM, [salt] = 100 mM, [HPTS] = 1 mM). The successful incorporation of metallacycles into the vesicle membrane was confirmed by FT-IR spectra, which showed strong peaks at $\sim$1650 cm^{-1} due to C=O (NH) of the

metallacycle (Fig. S19, ESI†). The combination was also verified by confocal fluorescence spectroscopy. Metallacycles **1–3** are all fluorescent, while the lipids are non-fluorescent, and so the appearance of fluorescent rings confirms the encapsulation of metallacycles into the vesicle membrane,[54] as shown in Fig. S20 (ESI†). The operating principle for assessing ion transport across the lipid is as follows. The metallacycle was added to the vesicle solution, and a pH gradient (ΔpH = 0.6, pH_{in} = 7.0, pH_{out} = 7.6) was produced across the EYPC bilayer by adding NaOH to the extravesicular solution. The metallacycle activity was implied by destruction of the resultant pH gradient between the interior and the exterior of vesicles, which was monitored through the change in the relative fluorescence of HPTS. Finally, the vesicles were lysed by adding Triton X-100 to obtain the maximum fluorescence intensity.

We first evaluated the transport activities of **1–3** to Cl^- using this HPTS assay. Traces from experiments at a metallacycle/lipid molar ratio of 1:75 are shown in Fig. 5a. The results showed that **1** containing hydroxyl groups was almost inactive, presumably because the polar and hydrophilic hydroxyl groups cover the surface of the metallacycle, thus leading to the low lipophilicity of **1** and reducing the insertion efficiency to the lipid.[50] In contrast, **2** functionalized with ethoxyl groups exhibited a moderate ion transport activity of 46%, and **3** with crown ether groups displayed the highest ion transport activity, reaching 93% of the maximum fluorescence intensity within 300 s
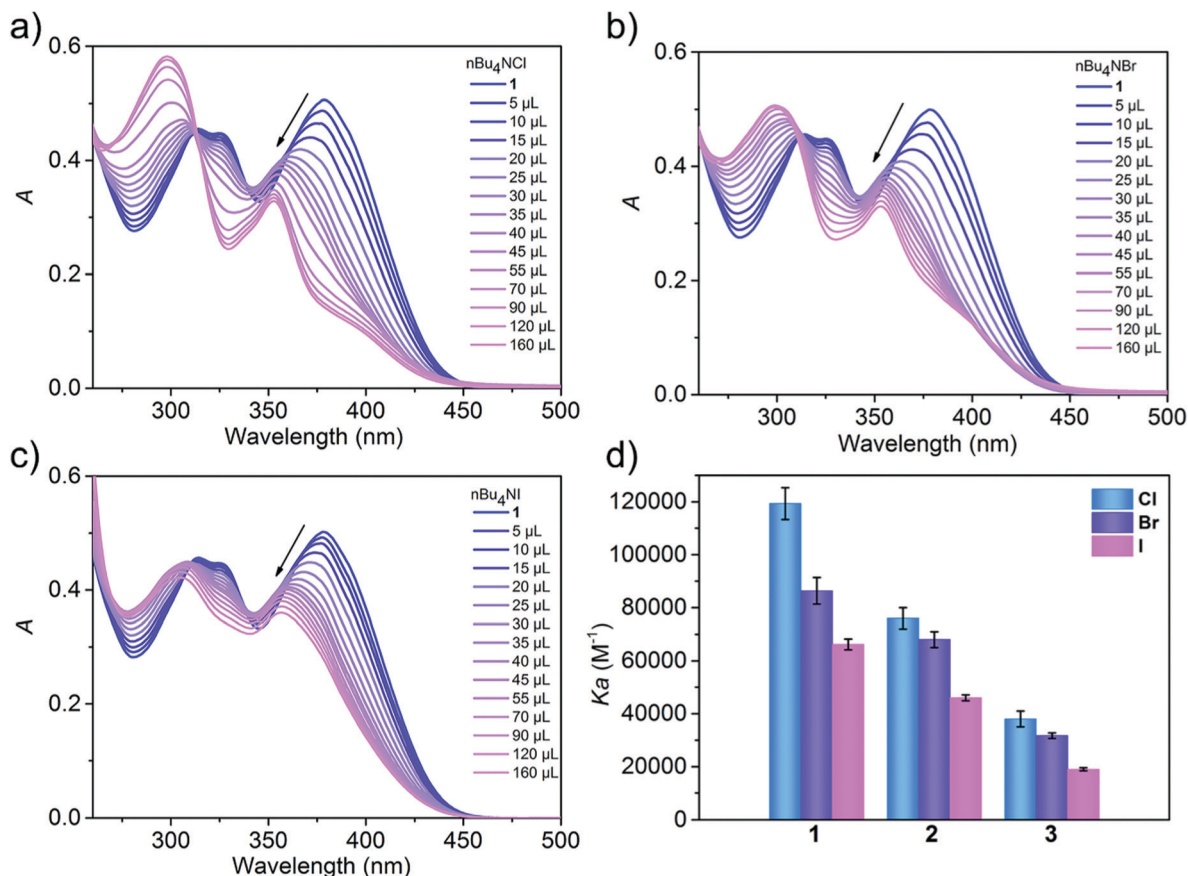
Fig. 4 (a–c) UV-vis spectra of metallacycle **1** with increasing concentrations of TBACl, TBABr and TBAI in CH_3CN. (d) Binding constants (K_a) of metallacycles **1–3** with TBACl, TBABr and TBAI.

(Fig. 5a). It is likely that the pendent –OR groups of (S)-1,1′-BINOL-based ligands have a significant effect on the transport activity of the assembled metallacycles.[50]

According to the dose–response curve shown in Fig. 5b and Fig. S21, (ESI†) the EC_{50} (the effective concentration required to

give half of the maximum response) values of **2** and **3** were calculated to be 8.9 and 1.5 μM, respectively. At this concentration, the molar ratios of **2**/lipid and **3**/lipid are 1 : 42 and 1 : 250, respectively, also indicating that **3** exhibited a good ion transport efficiency. We also examined the Cl^- transport
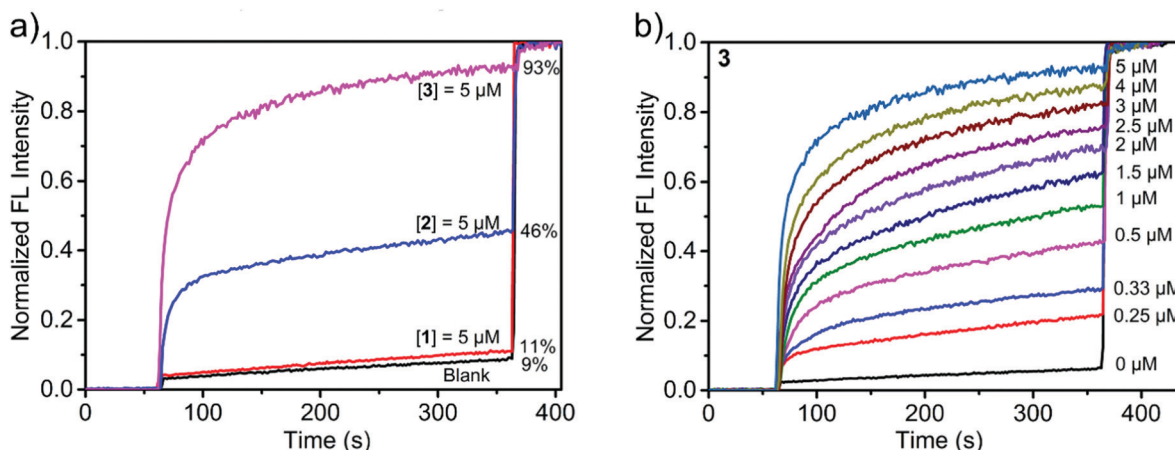

Fig. 5 (a) Ion-transport activities of metallacycles **1–3** determined by the HPTS assay and normalized fluorescence data for the HPTS assay after adding **1–3** to EYPC–LUVs (metallacycle : lipid = 1 : 75). Solution inside the liposome: 1 mM HPTS, 10 mM HEPES, and 100 mM NaCl. Solution outside the liposome: 10 mM HEPES and 100 mM NaCl, pH = 7.6. (b) Changes in the HPTS fluorescence intensities upon the addition of increasing concentrations of **3** to EYPC–LUVs.
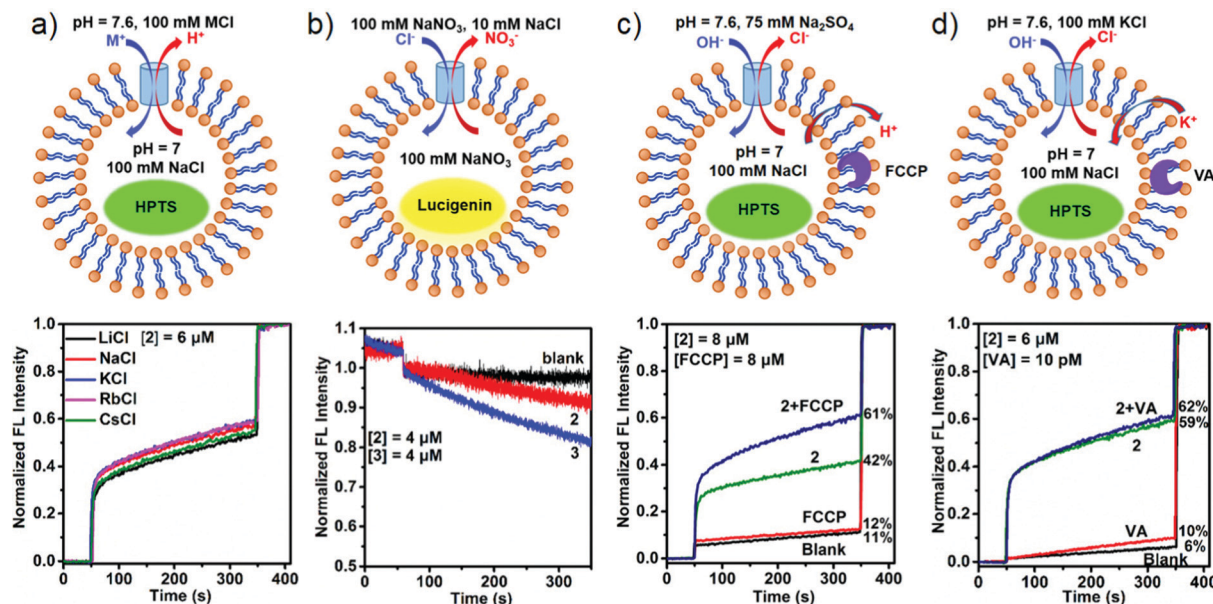
Fig. 6 (a) Cation selectivity evaluated by the HPTS assay. (b) Lucigenin assay using a chloride-sensitive lucigenin dye. (c) Comparison of the ion transport activity of **2** in the presence and the absence of FCCP. (d) Comparison of the ion transport activity of **2** in the presence and the absence of VA.

behaviors of subcomponents of metallacycles. When (S)-**L^2**, (S)-**L^3**, or $Zn(ClO_4)_2$ was employed in the transport process, no obvious ion-transport activity was detected in all cases in the HPTS transport assay (Fig. S21d, ESI†). In order to evaluate the influence of the fluorescence of metallacycles on the HPTS assay, we have performed control experiments, and the results showed that the fluorescence of metallacycles is very weak, and hence it is negligible compared with the fluorescence changes of HPTS in the transport process (Fig. S22 and S23, ESI†). Moreover, carboxyfluorescein (CF) assays indicated that the membrane integrity can be well retained in the presence of **2** and **3** (Fig. S24, ESI†).

The metallacycle-mediated ion transport mechanism was also studied. As shown in Fig. 6, four possible mechanisms (the H$^+$/M$^+$ antiport, the OH$^-$/A$^-$ antiport, the H$^+$/A$^-$ symport or the M$^+$/OH$^-$ symport) may cause the fluorescence intensity changes of HPTS, which was used to examine the ion transport activity. In order to explore the possible transport mechanism, a series of control experiments were performed on **2** and **3**. First, different alkali metal salts, namely, LiCl, NaCl, KCl, RbCl and CsCl, in the extravesicular solution were applied in the HPTS assay, and insignificant fluorescence intensity changes of HPTS were found in the **2**-mediated transport process, suggesting a little involvement of these cations in the transport (Fig. 6a). However, when **3** was used, different maximum intensities of fluorescence were produced by different metal salts within 300 s [LiCl (64%), NaCl (56%), KCl $\approx$ CsCl (51%), and RbCl (35%)] (Fig. S25, ESI†), indicating that the cations are involved in the ion transport with low selectivity. Second, the transport of Cl$^-$ was examined by the lucigenin assay, whose fluorescence emission at 505 nm is quenched by Cl$^-$.[59] Quenching was found upon the addition of NaCl to the extravesicular solution to produce a chloride gradient across the

lipid membrane. The fluorescence decrease was detected in the presence of both metallacycles (4 μM) with a decreased rate with **3** being faster than that with **2**, providing the direct proof of **2**/**3**-mediated Cl$^-$ transport into LUVs (Fig. 6b and Fig. S26, ESI†). The above two evidences implied that rather than the M$^+$/OH$^-$ symport or the M$^+$/H$^+$ antiport, either the H$^+$/Cl$^-$ symport or the OH$^-$/Cl$^-$ antiport mechanism is the main operational mechanism in **2**-mediated ion transport, but the mechanism of **3**-mediated ion transport cannot be identified by the two evidences clearly. Third, in order to further understand the transport mechanism of **2** (H$^+$/Cl$^-$ or OH$^-$/Cl$^-$) and **3** (both of four mechanisms), the proton carrier of FCCP (carbonyl cyanide 4-(trifluoromethoxy)phenylhydrazone) was employed to scrutinize the mechanism. After deducting the blank transport, the HPTS fluorescence increased by 1% in FCCP alone, 19% and 26% by adding **2** and **3** in the presence of FCCP (Fig. 6c and Fig. S27a, ESI†), respectively. This means that Cl$^-$ can be transported faster than H$^+$ or OH$^-$, indicating that **2** and **3** have a cooperative action with FCCP.[60] Finally, valinomycin (VA, a K$^+$ carrier) was also used in the HPTS assay with the extravesicular salt of K$^+$ to explore the transport mechanism further. It was found that the transport activities of **2** and **3** increased slightly ($\sim$3%) in the presence of VA, comparable to the difference between VA (10%) and blank (6%), indicative of no cooperation between metallacycles and VA (Fig. 6d and Fig. S27b, ESI†). In short, these results suggest that the transport rate of **2** is Cl$^-$ > H$^+$/OH$^-$ and that of **3** is Cl$^-$ > M$^+$ > H$^+$/OH$^-$.[61] Further studies are in great need to establish the detailed mechanism behind the formation of the transmembrane metallacycle pore and the anion transport activity.

The metallacycle-mediated anion transport by a channel mechanism was demonstrated in the single-channel planar bilayer conductance (PBC) experiment (Fig. 7). The bilayer
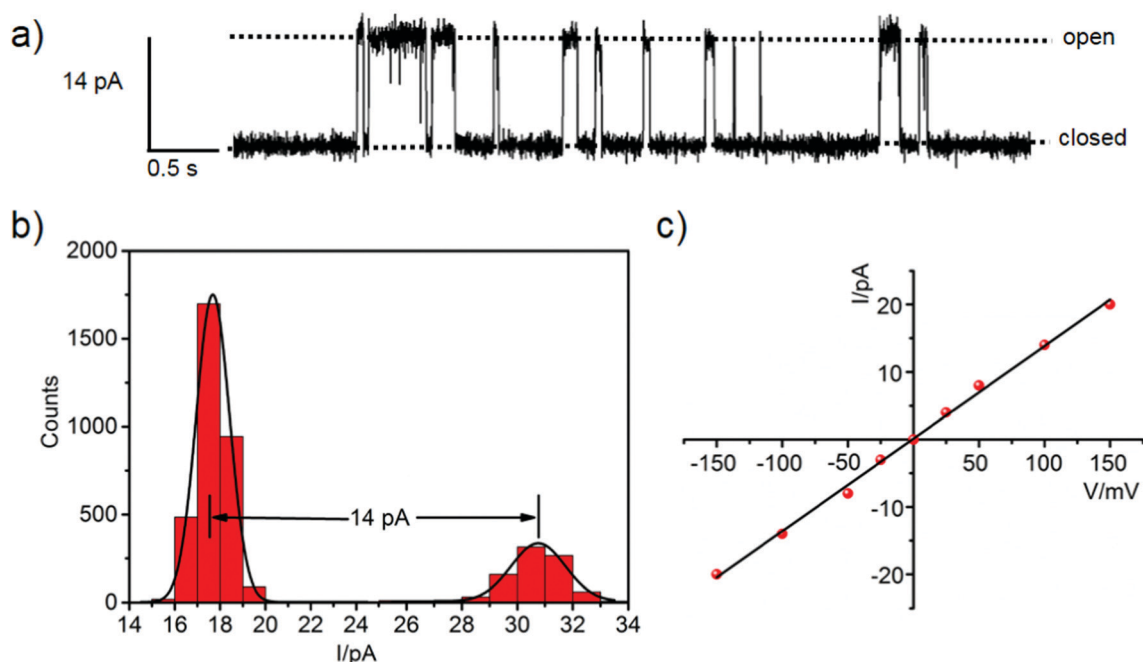
Fig. 7   (a) Current traces of metallacycle **2** at +100 mV in KCl solution (1.0 M). (b) A histogram of the currents at +100 mV. The data were fitted to two Gaussian distributions and the difference in ion current was measured. (c) *I/V* plots showing the average ion current flow from +150 to −150 mV.

composed of 1,2-diphytanoyl-*sn-glycero*-3-phosphocholine (DPhPC) was formed between two chambers containing the same solution, and metallacycle **2** in CH_3CN was added to one chamber (Fig. S28, ESI†). A potential was applied across the membrane to induce changes of the single-channel current profile with distinct open and closed states (Fig. 7a), which proved the metallacycle integrated to the bilayer and formed a single channel rather than acting as a carrier. A series of electric currents were recorded at different potentials in the range of ±150 mV (Fig. S29, ESI†). The single channel conductance was measured as 137 ± 3 pS from the linear relationship between the current and voltage (*I/V* plot, Fig. 7b and c). Hille analysis of the PBC data revealed the average diameter of the channel

formed by **2** to be ∼5.1 Å, close to the cavity diameter calculated by X-ray diffraction (Fig. 2b). Obviously, the PBC experiment demonstrated that the anions are indeed transmitted through the metallacycle channel.

Having established the channel activity of **2** and **3**, we tested their transport capability and selectivity toward other anions including Cl^-, Br^-, I^-, NO_3^- and ClO_4^-. In the HPTS-based experiments for determining the anion selectivity, the same sodium salts were used in both intra- and extravesicular solutions with a proton gradient by adding aqueous NaOH solution. From the determined EC_{50} values (Fig. 8 and S30–S34, ESI†), the anion transport abilities of both **2** and **3** decreased in the order $I^- > Br^- > NO_3^- > Cl^- > ClO_4^-$, which followed the
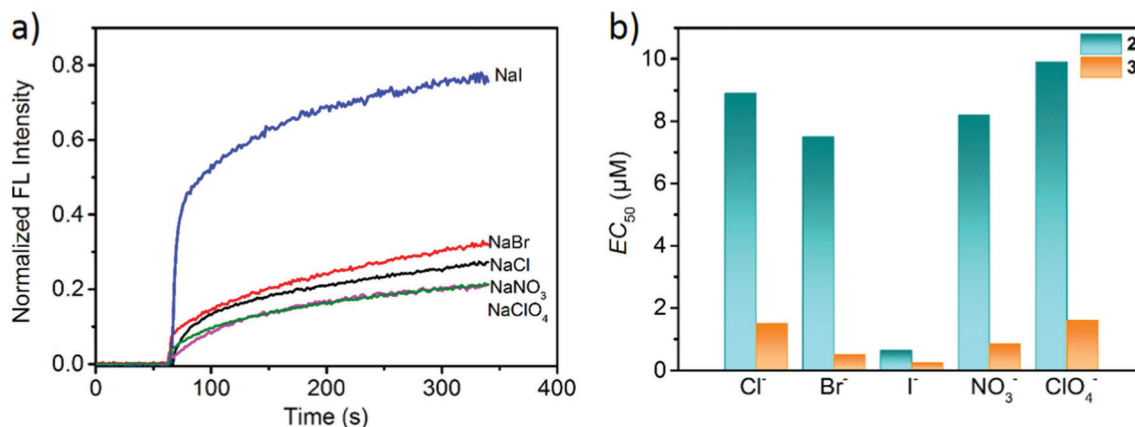

Fig. 8   (a) Transport activities toward Cl^-, Br^-, I^-, NO_3^- and ClO_4^- at a final concentration of 1 μM for **2** (**2** : lipid = 1 : 375). The background rates of I^- and ClO_4^- were subtracted. (b) The EC_{50} values for **2** and **3** mediated transport of Cl^-, Br^-, I^-, NO_3^- and ClO_4^- determined using the HPTS assay.

Hofmeister series.[62] Interestingly, metallacycle **2** displayed a high transport activity to I^- (EC_{50} = 0.64 μM), but low transport activities to Cl^-, Br^-, NO_3^- and ClO_4^-. The correlation between anion hydrophobicity and transport activity indicates that desolvation may be the rate-limiting factor in the ion transport process.[53] However, the transport rate of ClO_4^- is low as compared to their position in the Hofmeister series, which is probably attributed to the size/shape exclusion hindering the passage of the larger ClO_4^- through the rigid channel. Similar results have been reported in other systems.[42] Thus, both **2** and **3** can selectively transport anions and have a higher selectivity for I^- over other anions, as shown in Fig. 8. The I^-/X^- selectivity ratios that were obtained by comparing their EC_{50} values $[EC_{50}(X^-)/EC_{50}(I^-)]$ ranged from 11.7 to 15.4 for **2** (I^-/Cl^- = 13.9, I^-/Br^- = 11.7, I^-/ClO_4^- = 15.4, I^-/NO_3^- = 12.8) and from 2 to 6.4 for **3** (I^-/Cl^- = 6, I^-/Br^- = 2, I^-/ClO_4^- = 6.4, I^-/NO_3^- = 3.4). Therefore, compared to metallacycle **3**, **2** showed a much higher transport selectivity for I^- over other anions.

Narrow and relatively hydrophobic pore regions are a typical feature of biological channels[63] that facilitates the transport of polar species including both ions and polar molecules. Both **2** and **3** have a central pore size of ~6 Å, which is among the diameters of iodide ions (4.32 Å) and hydrated iodide (6.62 Å) and is considered as an ideal size for selective I^- permeation.[64] The selectivity among the anions ($I^- > Br^- > Cl^-$) follows the Hofmeister series, in which various phenomena including enzymatic activity and polymer conformation are affected by the polarizability of environmental anions.[65] The more polarizable I^- ions should face a lower activation barrier to entry into the hydrophobic interior of metallacycle **2**,[66,67] thus resulting in a faster transport rate than other anions.

By comparing our results and the literature report,[13,41] it is found that the activity of metallacycle **2** (EC_{50} = 0.17 mol% for I^-) is almost three times higher than that of Kim's system (EC_{50} > 0.5 mol%). To compare with Kim's excellently selective iodide channel,[41] the same HPTS assay conditions were applied to **2** (Fig. S35, ESI†) because the different experimental conditions make comparisons difficult. The resulting data displayed a highest influx rate of I^- (5.7×10^{-4} s^{-1}), and the slow transport was found to the other examined anions. On the basis of initial rate constants (Table S4, ESI†), the I^-/Cl^- and I^-/Br^- selectivities were calculated to be 20 and 5, respectively, comparable to those of Kim's (60 for I^-/Cl^- and 6 for I^-/Br^-) iodide channel (Table S5, ESI†). But the I^-/NO_3^- selectivity can reach 38 which is much higher than Kim's (1.8) ion channel.

Conclusions

In summary, we have developed a new system for the construction of well-defined metal–organic macrocycles with fine-tuning of pore microenvironments for iodide-selective transmembrane transport. Coordination reactions of metal ions with (S)-1,1′-BINOL-based bis[2-(hydrazonomethyl)pyridine] ligands produced three cationic Zn_4L_4 metallacycles, whose pore microenvironments involving cavity size and shape,

recognition site, and surface nature can be readily tuned through the deployment of ligands with different functionalities. After embedding into the lipid membranes, the metallacycle with hydrophilic hydroxyl groups cannot transport anions and the one with amphiphilic pentaethylene glycol can transport anions but with low selectivity. In marked contrast, the metallacycle featuring ethoxyl groups, having a suitable cavity size and shape, rich binding sites, and high-density hydrophobic surfaces, can efficiently transport I^- over other anions through a bilayer membrane, with the transport selectivities that are comparable or favorably comparable to those of the most selective supramolecular assemblies for I^- transport. This work demonstrated that novel artificial anion channels can be constructed from shape-persistent metal–organic assemblies by fine-tuning of the pore microenvironments, which would facilitate the rational design of practically useful synthetic channels for ion/molecule sensing and separation.

Conflicts of interest

The authors declare no competing financial interests.

Acknowledgements

References

1 B. Hille. *Ionic Channels of Excitable Membranes*, Sinauer Associates, MA, 3rd edn, 2001.

2 C. M. Armstrong and B. Hille, Voltage-Gated Ion Channels and Electrical Excitability, *Neuron*, 1998, **20**, 371–380.

3 J. T. Davis, P. A. Gale and R. Quesada, Advances in Anion Transport and Supramolecular Medicinal Chemistry, *Chem. Soc. Rev.*, 2020, **49**, 6056–6086.

4 T. M. Fyles, Synthetic Ion Channels in Bilayer Membranes, *Chem. Soc. Rev.*, 2007, **36**, 335–347.

5 E. N. W. Howe and P. A. Gale, Fatty Acid Fueled Transmembrane Chloride Transport, *J. Am. Chem. Soc.*, 2019, **141**, 10654–10660.

6 H. Li, H. Valkenier, L. W. Judd, P. R. Brotherhood, S. Hussain, J. A. Cooper, O. Jurček, H. A. Sparkes, D. N. Sheppard and A. P. Davis, Efficient, Non-Toxic Anion

Transport by Synthetic Carriers in Cells and Epithelia, *Nat. Chem.*, 2016, **8**, 24–32.

7 W. Guo, Y. Tian and L. Jiang, Asymmetric Ion Transport through Ion-Channel-Mimetic Solid-State Nanopores, *Acc. Chem. Res.*, 2013, **46**, 2834–2846.

8 L. A. Marchetti, L. K. Kumawat, N. Mao, J. C. Stephens and R. B. P. Elmes, The Versatility of Squaramides: From Supramo-lecular Chemistry to Chemical Biology, *Chem*, 2019, **5**, 1398–1485.

9 K. A. Muraglia, R. S. Chorghade, B. R. Kim, X. X. Tang, V. S. Shah, A. S. Grillo, P. N. Daniels, A. G. Cioffi, P. H. Karp, L. Zhu, M. J. Welsh and M. D. Burke, Small-Molecule Ion Channels Increase Host Defences in Cystic Fibrosis Airway Epithelia, *Nature*, 2019, **567**, 405–408.

10 Z.-L. Hu, M.-Z. Huo, Y.-L. Ying and Y.-T. Long, Biologi-cal Nanopore Approach for Single-Molecule Protein Sequencing, *Angew. Chem., Int. Ed.*, 2021, **60**, 14738–14749.

11 B. Roux, S. Bernèche and W. Im, Ion Channels, Permeation, and Electrostatics: Insight into the Function of KcsA, *Biochemistry*, 2000, **39**, 13295–13306.

12 Z. Sun, M. Barboiu, Y.-M. Legrand, E. Petit and A. Rotaru, Highly Selective Artificial Cholesteryl Crown Ether K^+-Channels, *Angew. Chem., Int. Ed.*, 2015, **54**, 14473–14477.

13 A. Roy, H. Joshi, R. Ye, J. Shen, F. Chen, A. Aksimentiev and H. Zeng, Polyhydrazide-Based Organic Nanotubes as Efficient and Selective Artificial Iodide Channels, *Angew. Chem., Int. Ed.*, 2020, **59**, 4806–4813.

14 C. Lang, X. Deng, F. Yang, B. Yang, W. Wang, S. Qi, X. Zhang, C. Zhang, Z. Dong and J. Liu, Highly Selective Artificial Potassium Ion Channels Constructed from Pore-Containing Helical Oligomers, *Angew. Chem., Int. Ed.*, 2017, **56**, 12668–12671.

15 C. Ren, J. Shen and H. Zeng, Combinatorial Evolution of Fast-Conducting Highly Selective K^+-Channels via Modularly Tunable Directional Assembly of Crown Ethers, *J. Am. Chem. Soc.*, 2017, **139**, 12338–12341.

16 M. R. Ghadiri, J. R. Granja and L. K. Buehler, Artificial Transmembrane Ion Channels from Self-Assembling Peptide Nanotubes, *Nature*, 1994, **369**, 301–304.

17 S. Matile, A. Som and N. Sordé, Recent Synthetic Ion Channels and Pores, *Tetrahedron*, 2004, **60**, 6405–6435.

18 X.-X. Gou, T. Liu, Y.-Y. Wang and Y.-F. Han, Ultrastable and Highly Catalytically Active N-Heterocyclic-Carbene-Stabilized Gold Nanoparticles in Confined Spaces, *Angew. Chem., Int. Ed.*, 2020, **59**, 16683–16689.

19 X. Zhang, X. Dong, W. Lu, D. Luo, X.-W. Zhu, X. Li, X.-P. Zhou and D. Li, Fine-Tuning Apertures of Metal–Organic Cages: Encapsulation of Carbon Dioxide in Solution and Solid State, *J. Am. Chem. Soc.*, 2019, **141**, 11621–11627.

20 C. Yuan, X. Wu, R. Gao, X. Han, Y. Liu, Y. Long and Y. Cui, Nanochannels of Covalent Organic Frameworks for Chiral Selective Transmembrane Transport of Amino Acids, *J. Am. Chem. Soc.*, 2019, **141**, 20187–20197.

21 K. Dey, M. Pal, K. C. Rout, H. Shebeeb Kunjattu, A. Das, R. Mukherjee, U. K. Kharul and R. Banerjee, Selective Molecular Separation by Interfacially Crystallized Covalent

Organic Framework Thin Films, *J. Am. Chem. Soc.*, 2017, **139**, 13083–13091.

22 Y. Tanaka, Y. Kobuke and M. Sokabe, A Non-Peptidic Ion Channel with K^+ Selectivity, *Angew. Chem., Int. Ed.*, 1995, **34**, 693–694.

23 P. Xin, P. Zhu, P. Su, J.-L. Hou and Z.-T. Li, Hydrogen-Bonded Helical Hydrazide Oligomers and Polymer That Mimic the Ion Transport of Gramicidin A, *J. Am. Chem. Soc.*, 2014, **136**, 13078–13081.

24 W. L. Huang, X. D. Wang, Y. F. Ao, Q. Q. Wang and D. X. Wang, Artificial Chloride-Selective Channel: Shape and Function Mimic of the ClC Channel Selective Pore, *J. Am. Chem. Soc.*, 2020, **142**, 13273–13277.

25 T. R. Cook and P. J. Stang, Recent Developments in the Preparation and Chemistry of Metallacycles and Metalla-cages via Coordination, *Chem. Rev.*, 2015, **115**, 7001–7045.

26 M. Yoshizawa, M. Tamura and M. Fujita, Diels-Alder in Aqueous Molecular Hosts: Unusual Regioselectivity and Effi-cient Catalysis, *Science*, 2006, **312**, 251–254.

27 C. Gutz, R. Hovorka, C. Klein, Q. Q. Jiang, C. Bannwarth, M. Engeser, C. Schmuck, W. Assenmacher, W. Mader, F. Topic, K. Rissanen, S. Grimme and A. Lutzen, Enantio-merically Pure [M₆L₁₂] or [M₁₂L₂₄] Polyhedra from Flexible Bis(pyridine) Ligands, *Angew. Chem., Int. Ed.*, 2014, **53**, 1693–1698.

28 J. Tessarolo, H. Lee, E. Sakuda, K. Umakoshi and G. H. Clever, Integrative Assembly of Heteroleptic Tetrahedra Con-trolled by Backbone Steric Bulk, *J. Am. Chem. Soc.*, 2021, **143**, 6339–6344.

29 M. D. Pluth, R. G. Bergman and K. N. Raymond, Proton-Mediated Chemistry and Catalysis in a Self-Assembled Supra-molecular Host, *Acc. Chem. Res.*, 2009, **42**, 1650–1659.

30 B. Mondal and P. S. Mukherjee, Cage Encapsulated Gold Nanoparticles as Heterogeneous Photocatalyst for Facile and Selective Reduction of Nitroarenes to Azo Compounds, *J. Am. Chem. Soc.*, 2018, **140**, 12592–12601.

31 W.-X. Gao, H.-J. Feng, B.-B. Guo, Y. Lu and G.-X. Jin, Coordination-Directed Construction of Molecular Links, *Chem. Rev.*, 2020, **120**, 6288–6325.

32 K. Li, L.-Y. Zhang, C. Yan, S.-C. Wei, M. Pan, L. Zhang and C.-Y. Su, Stepwise Assembly of Pd₆(RuL₃)₈ Nanoscale Rhom-bododecahedral Metal–Organic Cages via Metalloligand Strategy for Guest Trapping and Protection, *J. Am. Chem. Soc.*, 2014, **136**, 4456–4459.

33 J. Wei, L. Zhao, C. He, S. Zheng, J. N. H. Reek and C. Duan, Metal–Organic Capsules with NADH Mimics as Switchable Selectivity Regulators for Photocatalytic Transfer Hydrogena-tion, *J. Am. Chem. Soc.*, 2019, **141**, 12707–12716.

34 R. Kawano, N. Horike, Y. Hijikata, M. Kondo, A. Carné-Sánchez, P. Larpent, S. Ikemura, T. Osaki, K. Kamiya, S. Kitagawa, S. Takeuchi and S. Furukawa, Metal-Organic Cuboctahedra for Synthetic Ion Channels with Multiple Conductance States, *Chem*, 2017, **2**, 393–403.

35 X. Wei, G. Zhang, Y. Shen, Y. Zhong, R. Liu, N. Yang, F. Y. Al-mkhaizim, M. A. Kline, L. He, M. Li, Z.-L. Lu, Z. Shao and B. Gong, Persistent Organic Nanopores Amenable to

Structural and Functional Tuning, *J. Am. Chem. Soc.*, 2016, **138**, 2749–2754.

36 A. Satake, M. Yamamura, M. Oda and Y. Kobuke, Transmembrane Nanopores from Porphyrin Supramolecules, *J. Am. Chem. Soc.*, 2008, **130**, 6314–6315.

37 M. Jung, H. Kim, K. Baek and K. Kim, Synthetic Ion Channel Based on Metal–Organic Polyhedra, *Angew. Chem., Int. Ed.*, 2008, **47**, 5755–5757.

38 Y. J. Jeon, H. Kim, S. Jon, N. Selvapalam, D. H. Oh, I. Seo, C.-S. Park, S. R. Jung, D.-S. Koh and K. Kim, Artificial Ion Channel Formed by Cucurbit[*n*]uril Derivatives with a Carbonyl Group Fringed Portal Reminiscent of the Selectivity Filter of K$^+$ Channels, *J. Am. Chem. Soc.*, 2004, **126**, 15944–15945.

39 U. Devi, J. R. D. Brown, A. Almond and S. J. Webb, Pd(II)-Mediated Assembly of Porphyrin Channels in Bilayer Membranes, *Langmuir*, 2011, **27**, 1448–1456.

40 T. M. Fyles and C. C. Tong, Long-Lived and Highly Conducting Ion Channels Formed by Lipophilic Ethylenediamine Palladium(II) Complexes, *New J. Chem.*, 2007, **31**, 655–661.

41 B. P. Benke, P. Aich, Y. Kim, K. L. Kim, M. R. Rohman, S. Hong, I.-C. Hwang, E. H. Lee, J. H. Roh and K. Kim, Iodide-Selective Synthetic Ion Channels Based on Shape-Persistent Organic Cages, *J. Am. Chem. Soc.*, 2017, **139**, 7432–7435.

42 C. J. E. Haynes, J. Zhu, C. Chimerel, S. Hernández-Ainsa, I. A. Riddell, T. K. Ronson, U. F. Keyser and J. R. Nitschke, Blockable Zn$_{10}$L$_{15}$ Ion Channels through Subcomponent Self-Assembly, *Angew. Chem., Int. Ed.*, 2017, **56**, 15388–15392.

43 L.-L. Yan, C.-H. Tan, G.-L. Zhang, L.-P. Zhou, J.-C. Bünzli and Q.-F. Sun, Stereocontrolled Self-Assembly and Self-Sorting of Luminescent Europium Tetrahedral Cages, *J. Am. Chem. Soc.*, 2015, **137**, 8550–8555.

44 H. Wang, C.-H. Liu, K. Wang, M. Wang, H. Yu, S. Kandapal, R. Brzozowski, B. Xu, M. Wang, S. Lu, X.-Q. Hao, P. Eswara, M.-P. Nieh, J. Cai and X. Li, Assembling Pentatopic Terpyridine Ligands with Three Types of Coordination Moieties into a Giant Supramolecular Hexagonal Prism: Synthesis, Self-Assembly, Characterization, and Antimicrobial Study, *J. Am. Chem. Soc.*, 2019, **141**, 16108–16116.

45 C.-B. Huang, L. Xu, J.-L. Zhu, Y.-X. Wang, B. Sun, X. Li and H.-B. Yang, Real-Time Monitoring the Dynamics of Coordination-Driven Self-Assembly by Fluorescence-Resonance Energy Transfer, *J. Am. Chem. Soc.*, 2017, **139**, 9459–9462.

46 F.-R. Dai and Z. Wang, Modular Assembly of Metal–Organic Supercontainers Incorporating Sulfonylcalixarenes, *J. Am. Chem. Soc.*, 2012, **134**, 8002–8005.

47 X. Yan, T. R. Cook, J. B. Pollock, P. Wei, Y. Zhang, Y. Yu, F. Huang and P. J. Stang, Responsive Supramolecular Polymer Metallogel Constructed by Orthogonal Coordination-Driven Self-Assembly and Host/Guest Interactions, *J. Am. Chem. Soc.*, 2014, **136**, 4460–4463.

48 S. J. Lee and W. Lin, Chiral Metallocycles: Rational Synthesis and Novel Applications, *Acc. Chem. Res.*, 2008, **41**, 521–537.

49 K. Su, W. Wang, S. Du, C. Ji, M. Zhou and D. Yuan, Reticular Chemistry in the Construction of Porous Organic Cages, *J. Am. Chem. Soc.*, 2020, **142**, 18060–18072.

50 X. Hu, C. Yu, K. D. Okochi, Y. Jin, Z. Liu and W. Zhang, Phenylene Vinylene Macrocycles as Artificial Transmembrane Transporters, *Chem. Commun.*, 2016, **52**, 5848–5851.

51 O. V. Kulikov, R. Li and G. W. Gokel, A Synthetic Ion Channel Derived from a Metallogallarene Capsule That Functions in Phospholipid Bilayers, *Angew. Chem., Int. Ed.*, 2009, **48**, 375–377.

52 M. Boccalon, E. Iengo and P. Tecilla, Metal–Organic Transmembrane Nanopores, *J. Am. Chem. Soc.*, 2012, **134**, 20310–20313.

53 D. P. August, S. Borsley, S. L. Cockroft, F. della Sala, D. A. Leigh and S. J. Webb, Transmembrane Ion Channels Formed by a Star of David [2]Catenane and a Molecular Pentafoil Knot, *J. Am. Chem. Soc.*, 2020, **142**, 18859–18865.

54 Y. D. Yuan, J. Dong, J. Liu, D. Zhao, H. Wu, W. Zhou, H. X. Gan, Y. W. Tong, J. Jiang and D. Zhao, Porous Organic Cages as Synthetic Water Channels, *Nat. Commun.*, 2020, **11**, 4927.

55 A. L. Spek, Single-Crystal Structure Validation with the Program PLATON, *J. Appl. Crystallogr.*, 2003, **36**, 7–13.

56 B. D. Zdravkov, J. J. Čermák, M. Šefara and J. Janků, Pore Classification in the Characterization of Porous Materials: A Perspective, *Cent. Eur. J. Chem.*, 2007, **5**, 1158.

57 D. B. Hibbert and P. Thordarson, The Death of the Job Plot, Transparency, Open Science and Online Tools, Uncertainty Estimation Methods and Other Developments in Supramolecular Chemistry Data Analysis, *Chem. Commun.*, 2016, **52**, 12792–12805.

58 B. J. W. Steed, First- and Second-Sphere Coordination Chemistry of Alkali Metal Crown Ether Complexes, *Coord. Chem. Rev.*, 2001, **215**, 171–221.

59 B. A. McNally, A. V. Koulov, B. D. Smith, J.-B. Joos and A. P. Davis, A Fluorescent Assay for Chloride Transport; Iden-tification of a Synthetic Anionophore with Improved Activity, *Chem. Commun.*, 2005, 1087–1089.

60 S. V. Shinde and P. Talukdar, A Dimeric Bis(melamine)-Substituted Bispidine for Efficient Transmembrane H$^+$/Cl$^-$ Co-transport, *Angew. Chem., Int. Ed.*, 2017, **56**, 4238–4242.

61 N. Sakai and S. Matile, The Determination of the Ion Selectivity of Synthetic Ion Channels and Pores in Vesicles, *J. Phys. Org. Chem.*, 2006, **19**, 452–460.

62 K. D. Collins and M. W. Washabaugh, The Hofmeister Effect and the Behaviour of Water at Interfaces, *Q. Rev. Biophys.*, 1985, **18**, 323–422.

63 M. Yazdani, Z. Jia and J. Chen, Hydrophobic Dewetting in Gating and Regulation of Transmembrane Protein Ion Channels, *J. Chem. Phys.*, 2020, **153**, 110901.

64 E. R. Nightingale, Phenomenological Theory of Ion Solvation. Effective Radii of Hydrated Ions, *J. Phys. Chem.*, 1959, **63**, 1381–1387.

65 M. C. Gurau, S.-M. Lim, E. T. Castellana, F. Albertorio, S. Kataoka and P. S. Cremer, On the Mechanism of the Hofmeister Effect, *J. Am. Chem. Soc.*, 2004, **126**, 10522–10523.

66 Z. Qi, M. Sokabe, K. Donowaki and H. Ishida, Structure-Function Study on a de Novo Synthetic Hydrophobic Ion Channel, *Biophys. J.*, 1999, **76**, 631–641.

67 N. Madhavan, E. C. Robert and M. S. Gin, A Highly Active Anion-Selective Aminocyclodextrin Ion Channel, *Angew. Chem., Int. Ed.*, 2005, **44**, 7584–7587.